Rahman, B. M., Uthman, M., Quadir, A., Kejalakshmy, N., Markides, C. & Themistos, C. (2013). Low-loss Waveguides and Devices for Compact THz Systems. Proceedings of SPIE, 8716, doi: 10.1117/12.2017622

CITY UNIVERSITY LONDON

City Research Online

Low-loss Waveguides and Devices for Compact THz Systems

B M a Rahman, M Uthman, A Quadir, N Kejalakshmy, C Markides and C Themistos
City University London Northampton Square, London EC1V 0HB, UK

ABSTRACT

A rigorous full-vectorial modal solution approach based on the finite element method is used to find the propagation properties of THz waveguides. Design approaches are presented to reduce the modal loss. Design of several THz devices, including quantum cascade lasers, plasmonic waveguides, power splitters and narrow-band filters are also presented.

Keywords-THz waveguides; THz devices, finite element method**.**

1. INTRODUCTION

The terahertz (THz) region occupies a large portion of the electromagnetic spectrum, located between the microwave and optical frequencies and normally is defined as the band ranging from 0.1 to 10 THz. In recent years, this intermediate THz radiation band has attracted considerable interest, because it offers significant scientific and technological potential for applications in many fields, such as sensing [1], imaging [2] and spectroscopy [3]. However, waveguiding in this intermediate spectral region is a major challenge and strong dielectric and conductive losses in the terahertz frequency range have been a major problem for waveguiding. The conventional guiding structures exemplified by microstrips, coplanar striplines and coplanar waveguides [4] are highly lossy and dispersive. However, so far the most promising dielectric waveguides have been the use of photonic crystal fibers at terahertz frequencies [5, 6] and metal coated guides [7] at terahertz frequencies. In this paper, various types of practical dielectric and metal coated waveguides are evaluated including their modal loss and dispersion and design optimization of Quantum Cascade Lasers, MMI-based power splitters and narrow-band filters are also presented, by using full-vectorial finite element method [8].

2. PHOTONIC CRYSTAL FIBERS: THZ WAVEGUIDES

Dielectric waveguides in silica, silicon, polymer, and other semiconductors materials have been widely used at optical frequencies: however most of these materials are very lossy at the lower terahertz frequency range. So far most of the PCFs that have been considered have been fabricated from silica or non-silica glasses, due to their low loss in the optical frequency range, but the material loss of silica is prohibitively high at THz frequencies. However, only recently, Han et al. [5] have fabricated a PCF for THz using high-density polyethylene (HDPE) with modal loss values of 0.2 cm^{-1} and Goto et al. [6] have reported a PCF-like waveguide using Teflon tubes and filaments with loss values of 0.5 cm^{-1}, showing their potential.

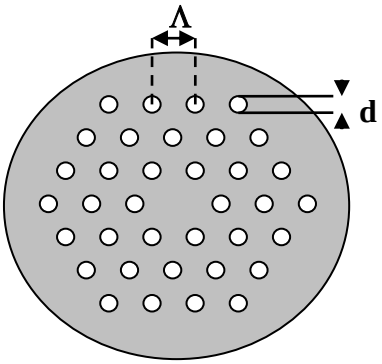

Figure 1. Cross section of a Photonic Crystal Fiber

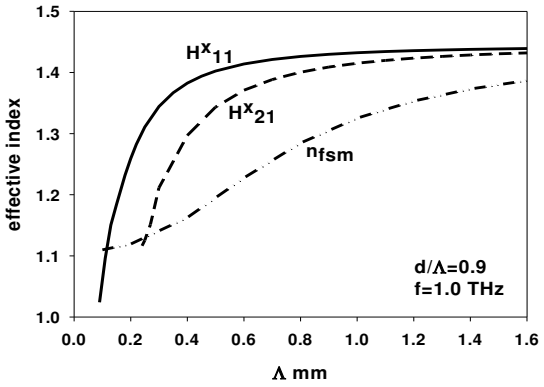

Figure 2. Variation of the effective indices with the pitch length, Λ.

A typical PCF cross section with a triangular array of holes is shown in Fig. 1. The structure predominantly consists of such periodic air-holes with diameter, d, and the pitch length between the two nearest holes is Λ. In this work, a refractive index value $n_g = 1.444$ is considered, at the operating frequency 1.2 THz (wavelength 0.25 mm). Variations of the effective indices for both the fundamental H^x_{11} and the second H^x_{21} modes for $d/\Lambda = 0.9$ are shown in Fig.2. It can be noted that for both the modes, the effective indices reduce monotonically as the pitch length is reduced. The variation of the n_{fsm} value with the pitch length is also shown by a chained line for $d/\Lambda = 0.9$ at 1.0 THz. The n_{fsm} represents a frequency dependent equivalent index of the perforated cladding region and this was calculated by solving a unit cell problem with periodic boundary conditions implemented around all the four sides. It can be observed that the effective index curve for the H^x_{21} mode crosses the n_{fsm} line at a pitch length, $\Lambda_c = 0.24$ mm, so when the pitch length is reduced below 0.24 mm, the second mode cannot continue to be guided. On the other hand, the effective index for the fundamental, H^x_{11} mode also crosses the n_{fsm} line, but at $\Lambda_c = 0.11$ mm. So, a PCF with $d/\Lambda = 0.9$ and pitch length between 0.11 mm to 0.24 mm would be strictly single moded. By controlling the d/Λ ratio and the pitch length the modal properties of such low-loss PCFs at THz operating frequency can easily be controlled.

The modal loss of a guided mode in a PCF is due to the combination of the material loss and the leakage loss. The material loss arises due to the complex refractive indices of the waveguide materials and the leakage loss arises due to the modal index being lower than the surrounding high index cladding regions. In this work, perfectly matched layers (PML) [9] are incorporated around the orthodox computational window. For this study a PCF with parameter $d/\Lambda=0.5$ is used. To consider the effect of the loss tangent, three different values of the n_i, (the imaginary part) have been considered. Figure 3 shows the loss mechanism in a PCF. In the absence of any material loss, for $n_i = 0$, the leakage loss is shown by a solid line. It can be observed that as the pitch length is reduced, the leakage loss increases almost linearly from a very low loss value. In the case of $n_i = 0.00119$, the total loss included both the leakage loss and the material loss, which is shown by a dashed line. At a higher pitch value, when the leakage loss is negligible, the total loss is mainly attributable to the material loss. Although, it can be observed that by reducing the pitch value below 0.2 mm, confinement in more lossy solid dielectric can be reduced, however, this figure also shows that the leakage loss (and bending loss, which is not shown here) of such waveguides will also be very high.

Since at present the available dielectric materials at THz frequencies are considerable lossy, a novel design approach is considered next, where a porous core PCF is considered. As the waveguides dimensions for THz frequency are considerable bigger than that for the optical wavelength, it would be relatively easy to fabricate such microstructured core. Two different d/Λ values are used for core (d/Λ_i) and cladding (d/Λ_o), and for cladding this value has to be smaller to have higher equivalent index in the core for wave guidance. Variation of the power fraction in the air-region of the porous core is shown in Fig.4. As shown in this figure, the power confinement can be increased to 35% in the low-loss air-holes of the cores, and additionally another 25% in the cladding air-holes [10], but this is not shown here. With this arrangement, more than 60% power can be in the low-loss air region which will reduce the modal loss by 60% for a more flexible dielectric waveguide structure.

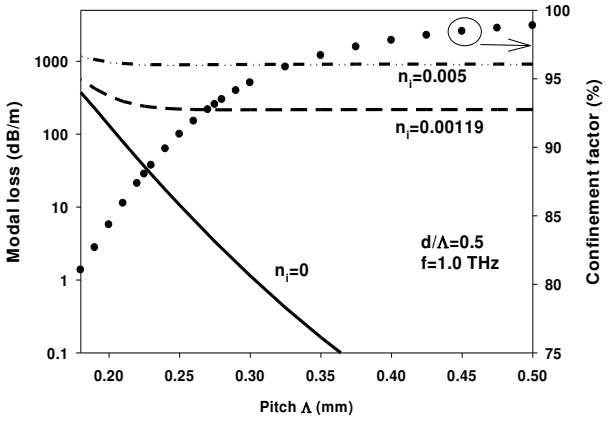

Figure 3. Material and leakage losses of PCF.

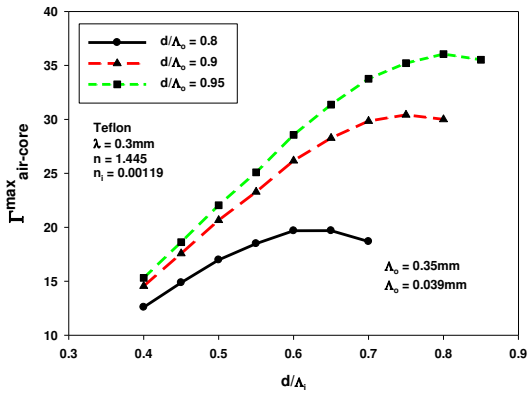

Figure 4. Variation of power confinement in the porous air-holes in the core region with the pitch length, Λ.

Amongst the various THz waveguides that have been suggested, the metal-clad waveguides supporting surface plasmon modes show the greatest promise as low-loss waveguides for use both in active components and as passive waveguides. Several waveguide structures incorporating metallic layers have been reported, such as low-loss and flexible hollow polycarbonate waveguide with copper and dielectric inner coatings, deposited by using a liquid chemistry approach [11].
A metal-coated hollow glass waveguide (HGW) [12] with an inner silver/polystyrene-coating, as shown in Fig.5, is considered for the better understanding of the various loss mechanisms and subsequently design optimization of a low-loss THz waveguide. For this waveguide the thickness of the silica tube (s) is taken as 0.5 mm and the bore radius (a) of the HGW as 2 mm. The thickness of the silver cladding (t) and polystyrene layer (p) are taken as t μm and p μm, respectively. The complex refractive index of the polystyrene, the silver metal cladding layers and the silica ring are taken as n_p=1.58 –j0.0036, n_m=308-j532 and n_s=1.96 –j0.0061, respectively at an operating frequency of 2.5 THz. At this frequency, as the air is also not absolutely loss-free, to represent this loss factor its complex refractive index is taken as 1.0 - j $1.1x10^{-6}$.

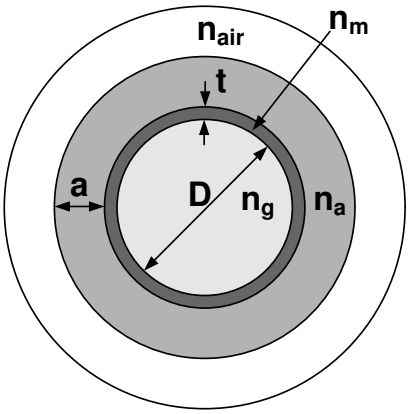

Figure 5. Metal-coated hollow glass waveguide

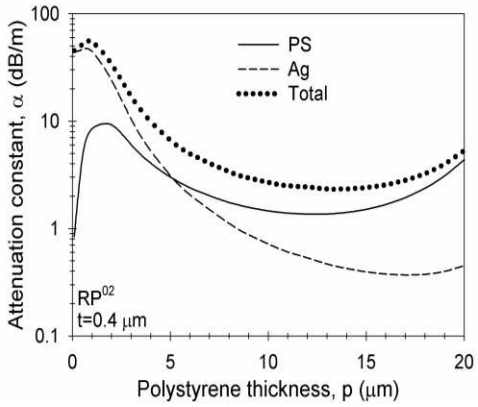

Figure 6. Attenuation constant with the polystyrene thickness, p, for t=0.4μm

There are two metal/dielectric interfaces, which can support surface plasmon modes (SPM), one the outer silver/silica boundary and the other at the inner silver/polystyrene (or air, when p = 0 μm) boundary. This waveguide supports two SPMs along these two metal/dielectric interfaces. The refractive indices of the inner and outer cladding materials being very different, the two SPMs have widely different propagation constants and they do not interact with each other. However, at the right and left hand sides of the metal/dielectric interfaces, when the same electric-wall boundary condition is imposed, the H_x field is forced to be zero at the metal boundary and no SPM exists. Another mode with the dominant H_y field, would form a similar SPM; however, at the left and the right interfaces. The H_y field profile of this mode is similar to the H_x field profile, but rotated by 90 degrees. These two modes have identical propagation constants and being degenerate, they can be superimposed to form radially polarized RP-like modes. The superposition of their field profiles indicates a rotationally symmetric profile similar to those reported for dielectric clad metal waveguides supporting surface plasmon modes at optical frequencies [13].
The loss values of the fundamental plasmonic mode increases with the PS thickness and not shown here. The attenuation characteristics of the RP^{02} mode, with the variation of the polystyrene thickness, for a silver thickness t = 0.4 μm, is shown in Fig. 6, where the loss contribution of the polystyrene and silver layers has also been examined. As can be seen from the above characteristics, the total attenuation shows a maximum and a minimum loss at a polystyrene thickness of about 1 μm and 13 μm, respectively. The attenuation curves due to the polystyrene and the silver layer exhibit similar trend with the total attenuation. Throughout the range of polystyrene thicknesses examined, the optical power confinement in the inner air-core is of the order of 99.9%, thus contributing a constant attenuation of about 0.25 dB/m. For a polystyrene thickness lower than 5 μm, the total attenuation is affected mainly due to the metal attenuation but as the polystyrene thickness increases above 5 μm the total attenuation is mainly governed by the loss in the polystyrene layer. This mode shows a greater promise to achieve low-loss guidance through a metal clad dielectric waveguides. It would also be easier to couple this mode since the field profile is also very close to a Gaussian shape [12]. The modal loss of this waveguide, when design is optimized, is significantly lower than most of the THz waveguides reported so far, as most of the power is being guided in the central air-hole region.

Next this novel approach is considered to design and optimize a low-loss rectangular core metal waveguide, as shown in Fig.7. If we consider its height and widths are different then the polarized modes will not be degenerate. In our more recent work [14], we have shown that similarly a polarization maintaining rectangular air-core dielectric-clad metal-coated waveguide can also be less lossy. A thin metal coating would support plasmonic modes, but these are relatively lossy. However, a Teflon coating on the gold layer can draws field away from the lossy conducting layer and loss may reduce considerably. Figure 8 shows the variation of the loss value with the Teflon thickness for the H^{x}_{12} mode in an air-core 1mm x 0.6 mm rectangular waveguide with 0.7 μm gold coating at 2.5 THz. It can be seen that at the optimum 21 μm Teflon thickness, the loss value can be 3.5 dB/m, one of the lowest reported so far [14]. The loss value can be further reduced by increasing the core dimension (W and h) but this would allow higher order modes to be guided. The evolution of third order mode for no Teflon coating (t_d = 0) to a near Gaussian profile for t_d =18 μm Teflon coating are shown as insets. The near Gaussian profile would be useful for efficient coupling of this mode from an external source. The 2-dimensional $H_x(x,y)$ profile for Teflon coated (with t_d = 18 μm) is also shown as another inset.

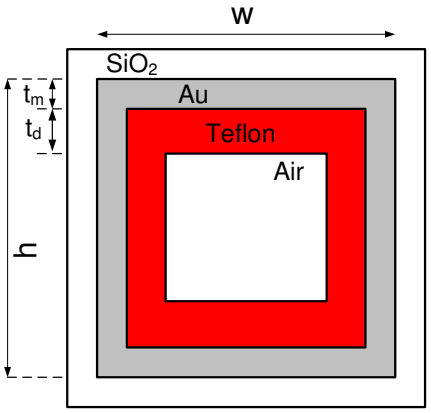

Figure 7. Low-loss rectangular core metal waveguide

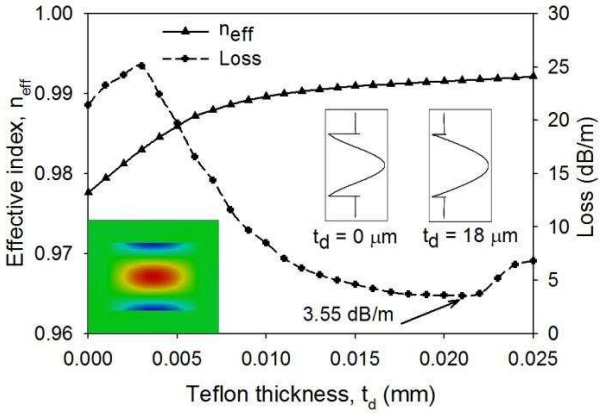

Figure 8. Effective index and loss with Teflon thickness for the Hx10 mode.

Moreover, the FDTD method is used to obtain the dispersion characteristics of the waveguide. A 2D formulation of the FDTD method with PML ABCs is used to study the electric field distribution along the axis of propagation of the waveguide. A Gaussian pulse was launched into the waveguide and the electric field at various points along the direction of propagation was monitored. The electric field distribution for an input profile, with spot size 80% and 90% of the width of the rectangular waveguide, sampled at 2.5THz using DFT, has been calculated but not presented here. The waveguide supports a propagating fundamental mode with high electric field value along the center of the waveguide. The propagating fundamental mode can be supported with small losses as the spot size of the input pulse is decreased to 90% and 80% respectively. After that threshold, as the spot size decreases there is a rapid decay in the electric field with significant losses and the plasmonic behavior of the waveguide rapidly deteriorates.

The normalized electric fields are plotted for an input source spot size 90% of the width of the waveguide (0.9mm) along the direction of propagation at two different locations, at z = 2 mm and 3 mm, and shown in Fig.9 by a solid and a dashed lines. The normalized electric field presents the difference in amplitude of the electric field with respect to the position of the monitor along the direction of propagation. Given the time-domain values of the normalized electric fields, the full-width half-maximum (FWHM) pulse width in ps for each of the monitors can be determined. The FWHM pulse spread is calculated at various points along the direction of propagation of the waveguide

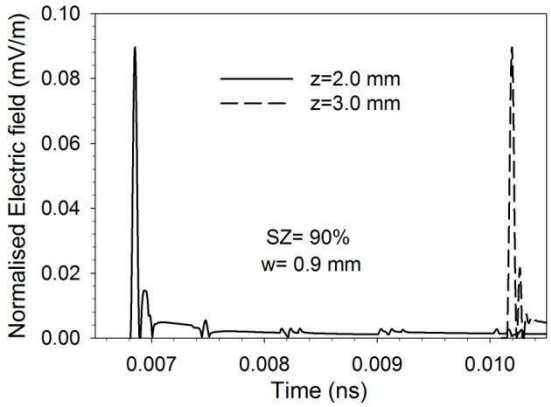

Figure 9. Normalized Electric field at 2mm and 3 mm along the direction of propagation

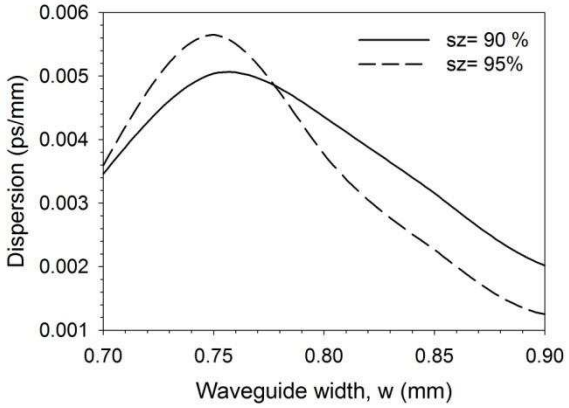

Figure 10. Full Wave Half Maximum pulse spread with propagation distance for different input pulse spot size.

The plasmonic waveguide dispersion (ps/mm) is presented in Figure 10 for various widths of the waveguide and for two different spot sizes of the input beam, 90% and 95% of the width of the waveguide. As the waveguide width is decreased the dispersion per unit length is increased reaching a maximum for a waveguide width of 0.75mm and when the input spot size is 95% of the width of the waveguide. Similarly, the waveguide dispersion is reaching a maximum for a waveguide width of 0.76mm when the input spot size is 90% of the width. As the width is decreased further down to 0.7mm the waveguide dispersion is also decreasing but a much slower rate, compared with the minimum waveguide dispersion values obtained for a 0.9mm waveguide width and spot size 90% and 95% of the width.

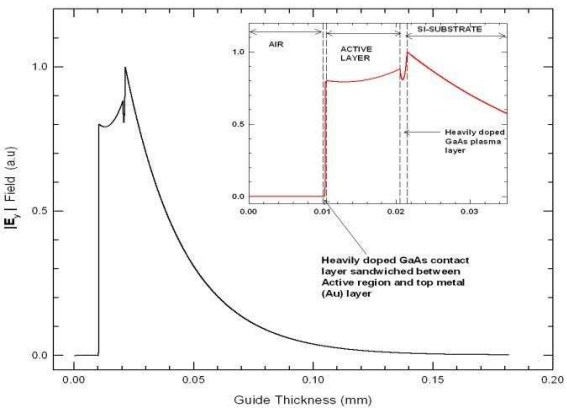

Figure 11. Field profile of $\mathbf{E}_y$ mode in a THz Quantum Cascade Laser. The field inside the confinement layers is shown on the inset.

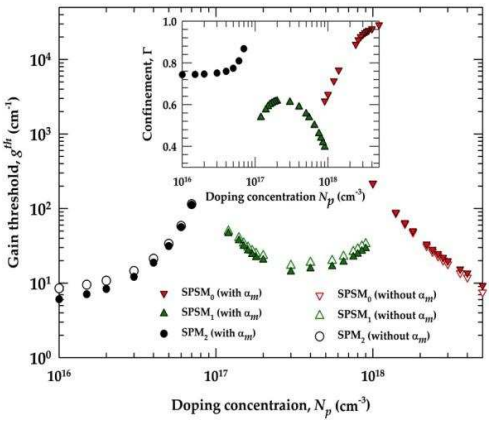

Figure 12. Gain threshold of several plasmonic modes.

Quantum cascading lasers [15] are emerging as efficient high power THz source for many important applications, such as imaging and sensing. However, for the THz frequency, the wavelength is large and it is not possible to grow the semiconductor materials comparable to the operating wavelength. For this reason, for THz QCL often smaller height needs to be considered and plasmonic confinement is used in that direction. The plasmonic confinement in the vertical direction is shown in Fig.11, which clearly shows the mode formation at the metal-dielectric interfaces. However, it is easily possible to have a wider guide, so mostly dielectric confinement is used in horizontal direction. The gain threshold for such QCL is shown in Fig.12. Because of the wider guides, the gain threshold difference between the fundamental and higher order (lateral) modes are very small. This allows possibility of mode hopping for any external changes. A

novel design approach is considered [16] using slotted upper metal clad, to enhance the gain threshold of the higher order modes. Fig. 13 clearly shows that gain threshold of the higher order modes are increased for slotted-electrode designs. For the future THz system, it is essential to design various integrated guided-wave components. In that spirit, it is shown here that a compact power splitter can b designed by using the MMI principle. In Fig. 14, it is shown here that an efficient power splitter can be designed by using a 35 μm long multimoded section [17].

Finally, a Terahertz frequency range band-stop filter for molecular sensing [18], where two 5 μm wide band-stop filter stubs with a length of 192 μm and 83 μm are placed at a 400 μm apart along the direction of propagation, as shown in the right inset of Fig.15, has been considered. Initially the above device has been simulated without a polysterene film on top of the metal layer, using the FDTD approach and the variation of the insertion loss with the frequency is presented in Fig.15. As can be seen from the above frequency response, the device exhibits two resonant frequencies due to the stubs at about 600 and 800 GHz, with a minimum insertion loss of about -55 and -30 dB.

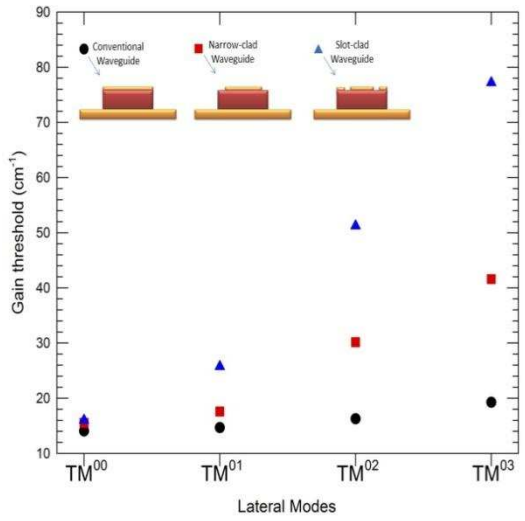

Figure 13. Gain Threshold of the lower order modes for different waveguides

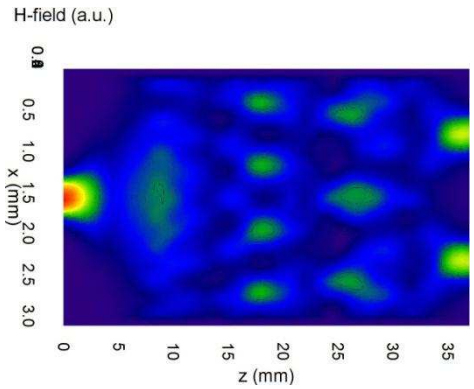

Figure 14. FDTD Simulation of the MMI 3dB coupler

Initially, the fundamental Quasi-TEM mode of the microstrip line, has been obtained using the FEM and the magnetic H_x field profile of the above mode is presented as inset in Fig.16 The effective index and attenuation of the above mode were found to be 1.803 and 44.59 (dB/mm), respectively. The effect on the propagation characteristics of the device of a polysterene layer along the top of the metal layer has then been examined, using the FEM. For a polysterene thickness of 0.1 μm the effective index and attenuation constant of the device were found be 1.76 and 35.21 (dB/mm), respectively, thus slightly lower compared with the corresponding values obtained for the plain metallic structure. However, as the polysterene thickness increases, both the effective index and the attenuation increase and for a thickness of 0.5 μm of the above material the loss level reaches the value obtained for the structure without the polysterene film. As the polysterene thickness further the attenuation increase much above the corresponding value obtained for the structure without the above film deposition (not shown here), and therefore, it can be concluded that attenuation reduction of the above device can only be achieved for a very thin polysterene film deposition.

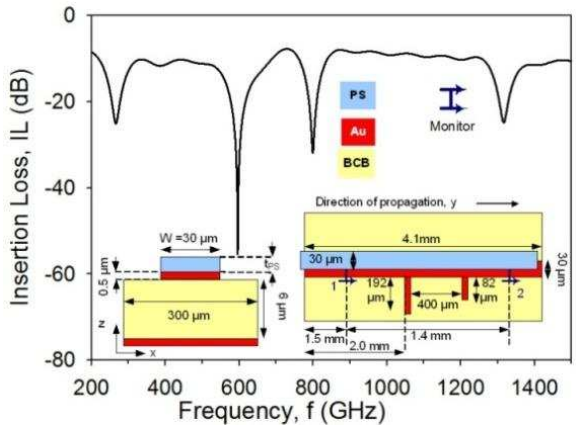

Figure 15. Insertion Loss with frequency for the microstrip filter

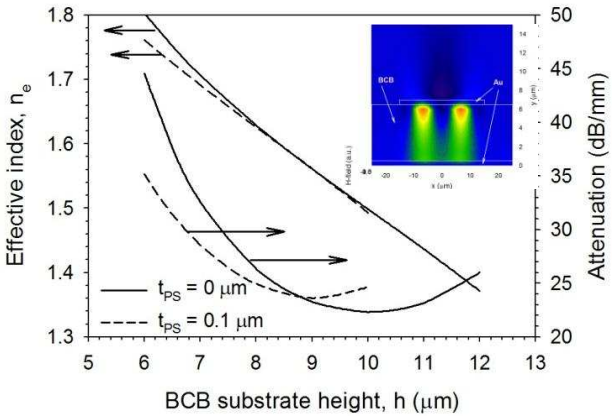

Figure 16. Variation of the effective index and attenuation with BCB substrate height of the microstrip line. (mode shown as inset)

The BCB substrate height, h, has then been varied and the effective index and attenuation of the microstrip structure with no polysterene layer on top of the metal and that with a 0.1 μm film thickness of the above material have been examined and presented in Fig.16. As can be seen from the above characteristics, as the substrate height increases both the effective index and the attenuation decrease, with the corresponding values of the structure with the polysterene film being lower than those obtained for the device without it. At a substrate height of about 9 μm, the above corresponding values are about the same for both the structures examined. However, the device with the polysterene film exhibits minimum attenuation at the above substrate height and as the substrate height increases further the attenuation of the structure with the polysterene layer becomes higher than that obtained for the structure without the above material.

3. CONCLUSION

A finite-element approach, based on a full-vectorial **H**-field formulation, has been used to study the detailed modal properties of dielectric and metal clad waveguides operating in the THz frequency range. It is also shown here that by using porous core the effect of material loss can be reduced significantly. It is also shown by using a thin but optimized dielectric over-layer plasmonic loss in a hollow-core waveguide can also be reduced. It is also shown here that by using a novel slot-type electrode, the differential loss of the higher order modes can be significantly increased to reduce mode hopping. Finally, simple guided-wave devices such as power splitters and band-pass filters are also presented here buy using the FDTD approach. The design approach used here can be extended to optimize not only THz waveguides but also more advanced guided-wave devices for possible THz integrated circuits (TIC) of the future.

REFERENCES

[1] R. H. Jacobsen, D. M. Mittleman, and M. C. Nuss, "Chemical recognition of gases and gas mixtures with terahertz waves," Optics Lett., **21**, no.24, pp. 2011-2013, 1996.

[2] Q. Chen, Z. Jiang, G. X. Xu, and X. C. Zhang, "Near-field terahertz imaging with a dynamic aperture," Optics Lett., **25**, no.15, pp.1122-1124, 2000.

[3] J. Q. Zhang and D. Grischkowsky, "Waveguide terahertz time-domain spectroscopy of nanometer water layers," Optics Lett., **29**, no.14, pp.1617-1619, 2004.

[4] M. Y. Frankel, S. Gupta, J. A. Valdmanis and G. A. Mourou, "Terahertz attenuation and dispersion characteristics of coplanar transmission-lines," IEEE Trans. Microwave Theory Tech., **MTT-39**, no.6, pp.910-916, 1991.

[5] H. Han, H. Park, M. Cho, and J. Kim, "Terahertz pulse propagation in plastic photonic crystal fiber," Appl. Phys. Lett, **80**, no.15, pp.2634-2636, 2002.

[6] M. Goto, A. Quema, H. Takahahi, S. Ono, and N. Sarukura, "Teflon photonic crystal fiber as terahertz waveguide," Jpn. J. Appl. Phys, Part 2 **43**, L317-L319, 2004.

[7] R. W. McGowan, G. Gallot, and D. Grischkowsky, "Propagation of ultrawideband short pulses of Terahertz radiation through submillimeter diameter circular waveguides," Opt. Lett, vol. **24**, no. 20, pp. 1431-1435, Oct 1999.

[8] B. M. A. Rahman and J. B. Davies, "Finite-element analysis of optical and microwave waveguide problems," Trans. Microwave Theory Tech, **MTT-32**, no.1, pp.20-28, 1984.
[9] N. Kejalakshmy, B. M. A. Rahman, A. Agrawal, T. Wongcharoen and K.T.V. Grattan, "Characterization of Single-Polarization Single-Mode Photonic Crystal Fiber using Full-Vectorial Finite Element Method," Appl. Phys. B, **93**, pp. 223-230, 2008.
[10] M Uthman et al, Design and characterization of low-loss porps-core photonic crystal fiber, IEEE Photonics J, vol. 4, no. 6, pp.2314-2325, Dec 2012.
[11] J. A. Harrington, R. George, P. Pederson, and E. Mueller, "Hollow polycarbonate waveguides with inner Cu coatings for delivery of terahertz radiation," Opt Express, vol. **12**, no.21, pp. 5263-5268, Oct. 2004.
[12] C. Themistos, B. M. A. Rahman, M. Rajarajan, K. T. V. Grattan, B. Bowden, and J. A. Harrington, "Characterization of Silver/Polystyrene (PS)-coated hollow glass waveguides at terahertz frequency," J. Lightwave. Technol., vol. **25**, no. 9, September 2007.
[13] C. Themistos, B. M. A. Rahman, and K. T. V. Grattan, "TM/TE modal solution for sub-micron lossy metal-clad optical fibers," Proc. Inst. Electr. Eng. – Optoelecton., vol. **145**, no. 3, pp. 171-177, Jun 1998.
[14] B.M.A. Rahman, A. Quadir, H. Tanvir and K.T.V. Grattan, "Characterization of Plasmonic Modes in a Low-Loss Dielectric-Coated Hollow Core Rectangular Waveguide at Terahertz Frequency," IEEE Photonics Journal, vol.3, pp.1054-1066, 2011.
[15] J. Faist, F.Capasso, D. L. Sivco, C. Sirtori, A. L. Hutchison, A. Y. Cho, "Quantum cascade laser," Science, vol.**264**, pp. 553-556, 1994.
[16] H. Tanvir, B.M.A. Rahman and K.T.V. Grattan, "Impact of "Ghost" Mode Interaction in Terahertz Quantum Cascade Lasers," IEEE Photonics Journal, vol.3, pp.926-935, 2011
[17] C. Markides, C. Themistos, H. Tanvir, B.M.A. Rahman, and K.T.V. Grattan, "Multimode Interference 3dB splitters in hollow core metallic waveguides for low loss THz wave transmission", Accepted in J. Selected Topics in Quantum Electron. (Manuscript ID: JSTQE-CON-CTTPA-04351-2012)
[18] J. Cunningham, C. Wood, A. G. Davies, I. Hunter, E. H. Linfield, and H. E. Beere, "Terahertz frequency range band-stop filters," Applied Physics Letters, vol.86,p.213503,2005